YALE JOURNAL OF BIOLOGY AND MEDICINE 91 (2018), pp.215-223.

ORIGINAL CONTRIBUTION

YJBM

Vibroacoustographic System for Tumor Identification

Peter A. Pellionisz[a,b,c,d,e,1], Nikan K. Namiri[c,d,1], Gregory Suematsu[c], Yong Hu[c], Ameet Braganza[c], Khuzaima Rangwalla[c], Daniel J. Denson[f], Karam Badran[b,c], Nathan C. Francis[c], Ashkan Maccabi[c,d], George Saddik[c,d], Zachary Taylor[b,c,d], Maie A. St. John[a,b,e], and Warren S. Grundfest[c,d,*]

[a]Department of Head and Neck Surgery, David Geffen School of Medicine at UCLA, Los Angeles, CA; [b]UCLA Head and Neck Cancer Program, David Geffen School of Medicine at UCLA, Los Angeles, CA; [c]Department of Bioengineering, Henry Samueli School of Engineering and Applied Sciences, UCLA, Los Angeles, CA; [d]Center for Advanced Surgical and Interventional Technology at Department of Surgery, David Geffen School of Medicine at UCLA, Los Angeles, CA; [e]Jonsson Comprehensive Cancer Center, David Geffen School of Medicine at UCLA, Los Angeles, CA; [f]Department of Physiological Sciences, UCLA, Los Angeles, CA

Oral and head and neck squamous cell carcinoma (OSCC†) is the sixth most common cancer worldwide. The primary management of OSCC relies on complete surgical resection of the tumor. Margin-free resection, however, is difficult given the devastating effects of aggressive surgery. Currently, surgeons determine where cuts are made by palpating edges of the tumor. Accuracy varies based on the surgeon's experience, the location and type of tumor, and the risk of damage to adjacent structures limiting resection margins. To fulfill this surgical need, we contrast tissue regions by identifying disparities in viscoelasticity by mixing two ultrasonic beams to produce a beat frequency, a technique termed vibroacoustography (VA). In our system, an extended focal length of the acoustic stress field yields surgeons' high resolution to detect focal lesions in deep tissue. VA offers 3D imaging by focusing its imaging plane at multiple axial cross-sections within tissue. Our efforts culminate in production of a mobile VA system generating image contrast between normal and abnormal tissue in minutes. We model the spatial direction of the generated acoustic field and generate images from tissue-mimicking phantoms and *ex vivo* specimens with squamous cell carcinoma of the tongue to qualitatively demonstrate the functionality of our system. These preliminary results warrant additional validation as we continue clinical trials of *ex vivo* tissue. This tool may prove especially useful for finding tumors that are deep within tissue and often missed by surgeons. The complete primary resection of tumors may reduce recurrence and ultimately improve patient outcomes.

*To whom all correspondence should be addressed: Warren S. Grundfest, MD, Department of Bioengineering, 4121H Engineering V, Los Angeles, CA 90095-1624; Tel: 310-794-5550, Fax: 310-794-5956, Email: warrenbe@seas.ucla.edu.

†Abbreviations: VA, vibroacoustography; TMP, tissue-mimicking phantom; ARF, acoustic radiation force; PVA, polyvinyl alcohol; PZT, lead zirconate titanate; OSCC, oral and head and neck squamous cell carcinoma, HNSCC, Head and neck squamous cell carcinoma.

Keywords: tumor imaging, intraoperative imaging, head and neck cancer

Author Contributions: [1]These authors contributed equally to this work. PAP: Validation, investigation, data curation, writing–original draft, and writing–review and editing. NKN: Validation, investigation, data curation, writing–original draft, and writing–review and editing. GS: Validation, investigation, data curation, writing–original draft, and writing–review and editing. YH Validation, investigation, data curation. AAB: Data curation, formal analysis, resources. KR: Data curation, resources. DD: Resources. KB: Data acquisition. NF: methodology, software, validation, formal analysis, resources. AM: methodology, software, validation, formal analysis, resources. GS: methodology, software, validation, formal analysis, resources. ZDT: Conceptualization, methodology, software, validation, formal analysis, resources, data curation, writing–original draft, writing–review and editing, visualization, supervision, project administration, and funding acquisition. WG: Conceptualization, methodology, supervision, project administration, and funding acquisition. MASJ: Conceptualization, methodology, validation, formal analysis, investigation, resources, data curation, writing–original draft, visualization, supervision, project administration, and funding acquisition.

INTRODUCTION

Head and neck squamous cell carcinoma (HNSCC) is the sixth most common neoplasia worldwide [1]. Nearly 70,000 new cases of oral and squamous cell carcinoma (OSCC) will be diagnosed this year, and despite focused research on conventional therapies, less than 50 percent of patients with advanced OSCC will survive over one year after diagnosis [2]. The major cause of these head and neck cancer-related deaths is persistent or recurrent disease [3–5]. It is challenging to remove the entirety of a tumor in the primary operation since many tumors have heterogeneous invasion deep to the surface that is not immediately apparent to the surgeon [6]. Furthermore, there is no standard tool for surgical image-guidance during oncologic procedures [7]. Recent results are promising in the domain of optical imaging but the limited penetration and scattering of light through tissue confines these techniques to the surface at best. This is especially troubling since, for example in floor of mouth tumors, the deep margin is the most common inadequate margin [8]. Larger deep surgical margins are recommended, yet aggressive resection may lead to adverse results including loss of voice, swallowing and speech problems, and anatomic deformities.

In order to define the edges of tumors, the surgeon largely relies on visual and tactile feedback with additional spot biopsy and frozen section. The major improvements in several imaging modalities (*i.e*., X-rays, ultrasound, MRI) have transformed modern oncologic surgery, yet there is still no consensus regarding the size of adequate margins [9–12]. The uniform identification of true boundaries is difficult since removal of the minimum necessary amount of tissue varies based on the experience of surgeon and pathologist, and the location of the tumor. Fortunately, the ongoing development and application of tools that produce visual guidance to the surgeon are closer than ever to the actualization of real-time image-guided surgery [13,14]. The majority of these imaging systems quantify various interactions of electromagnetic radiation with body tissues or fluid [15]. A notable exception, however, is ultrasound imaging and its derivatives. Conventional ultrasound relies on differences in the impedance of tissues to incoming waves and produces images defined by the acoustic properties of tissue [16]. Unfortunately, ultrasound is limited due to the similar acoustic impedance of tumor and healthy tissue and results in low contrast in delineating margins [17].

A more sophisticated approach to conventional ultrasound is vibroacoustography (VA), in which an image is produced from the amplitude and phase of the detected acoustic emissions of targeted tissue after exposure to a unique, low frequency acoustic radiation force (ARF) [18–20]. The acoustic force is generated by a low frequency wave (kHz), produced by two high frequency waves (MHz) that mix at a common focal point, and is able to penetrate deep within the surface of tissue. The produced lower frequency wave compresses and relaxes the tissue, eliciting a signal as a function of the target's mechanical properties (*i.e*., elastic modulus and viscosity) [21–23]. In our previous work, we report how differences in the stiffness of tissue types can be estimated using an acoustic perturbation from the localized acoustic force of VA [24,25]. The relevance is that the mechanical properties of a tissue are closely related to the inherent pathological state [26]. Thus, VA may identify areas based on quantitative measurements of the stiffness and viscous properties of tissue and aid in characterizing deep tissue masses (*e.g*., breast and prostate cancer, and localization of lymph nodes) due to the increased stiffness in these neoplastic tissues [27–30].

In this work we aim to develop a complementary tool that can provide depth dependent structural information in order to identify subcutaneous pockets of tumor. We aim to model the acoustic stress field that will be produced from a differential voltage across our transducer's elements, by using a multiphysics simulation. Then, we will construct a mobile system that measures the viscoelastic properties of tissue in order to delineate tumor from adjacent non-tumor. For proof of principle, tissue phantoms and *ex vivo* specimens relevant to clinical disease will be imaged. OSCC will be the pilot cancer for the characterization and validation of our system since these tumors are easily accessible in the clinical setting. This application also aligns with our ultimate goal of using this technology in the operating room. The results we obtain from querying OSCC are intended to lay the groundwork for future *in vivo* clinical investigations.

MATERIALS AND METHODS

Vibroacoustography (VA) Theory

The technique utilizes two non-destructive sinusoidal ultrasonic tones generated at slightly different frequencies in order to image tissue with a low kHz beat frequency (*i.e*. difference frequency). The signals are sent from a curved transducer, which can be positioned up to 6 cm beneath the superficial layer of tissue. The resulting acoustic stress field produces an ARF at the difference frequency between the two original tones, which perturbs the target tissue. Specifically, the difference frequency is produced upon mixing the two continuous sinusoids and creating an envelope, through superposition, containing the two original waves. The low frequency ARF at the difference frequency can be localized within or on the surface of the targeted lesion and permits measurable relaxation of the tissue with resultant omnidirectional

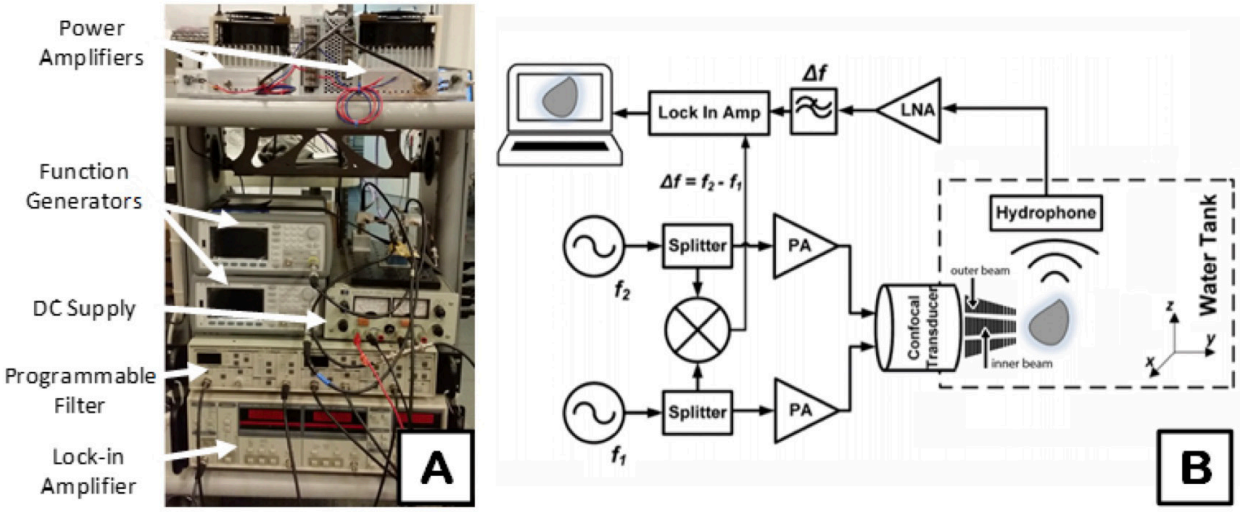

Figure 1. Vibroacoustography system schematic and design. **A**) System transceiver with labeled components, **B**) The system possesses function generators (f_1 and f_2) for creating the ultrasonic tones of difference frequency (Δf), 3dB splitters to divide the signals, mixer to mix the two split signals for a reference in the Lock-in amplifier, power amplifiers (PAs) to augment the input signals to the transducer, low noise amplifier (LNA), among other designated components.

emissive acoustic waves [18,19,21,22,31]. The tissue's emissive acoustic response, a function of the tissue's mechanical (*i.e.* viscoelastic) properties, is detected by a sensitive hydrophone coupled to the tissue. The amplitudes of tissue emissions are obtained and transformed into pixel values to create a spatially-accurate image. The phase of the tissue's emitted wave can also be correlated to the relative differences in viscoelastic properties of the probed volume [32,33].

System Simulation

We will use COMSOL (COMSOL Multiphysics, Stockholm, Sweden) to produce a simulation of the ARF at the focal point of the two beams from the inner and outer element of the transducer. Two MHz beams were produced from each element and directed into a control volume containing deionized water. The surface of the transducer was immersed into the control volume and each of its elements simulated with differential frequencies (*i.e.* f_1 and f_2, where f_1-f_2 = Δf). The difference frequency (*i.e.* Δf) was parameterized as 38 kHz, our current imaging frequency. The electric potential profile, measured in Volts, across each element was then measured by the software to identify any instances of overdriving of the PZT elements, which could potentially result in permanent displacement of the crystal structure and non-uniform mechanical stimulation. The acoustic beam patterns from each element were then modeled through the control volume. The curvature of the transducer was set to 5.9 cm based on current system design and thus a maximum acoustic stress field was expected at this focal distance.

System Design

The desired beat frequency of the acoustic stress is created by programming two offset MHz ultrasonic tones. The respective tones are created with two function generators (Keysight 33220A, Santa Clara, CA). Their output signal is coupled into a 3dB splitter (Minicircuits, Inc. Brooklyn, NY) that separates each tone into (1) each element of the confocal VA transducer with inner and outer layers and (2) a mixer (Minicircuits, Inc. Brooklyn, NY). Before reaching the two elements of the transducer, the signals are driven by power amplifiers (PAs) (AR Modular, Inc. Bothell, WA), as depicted in Figure 1A. The mixed signals are sent to a Lock-in Amplifier (SRS 844, Stanford Research Systems, Inc. Sunnyvale, CA) and function as a reference for modulation of the acoustic emission signal from the imaged samples (Figure 1A). The transducer is fabricated using two confocal layers of PZT that permit each MHz tone to be transduced separately within the same transducer. Furthermore, each MHz tone meets at a shared focal point. The confocal transducer is immersed within an ultrasound tank that uses water as a coupling agent (Figure 1B).

The imaged sample emits an acoustic response at the same ARF difference frequency used for stimulation. Next, a highly sensitive hydrophone (TC4014-5, Teledyne

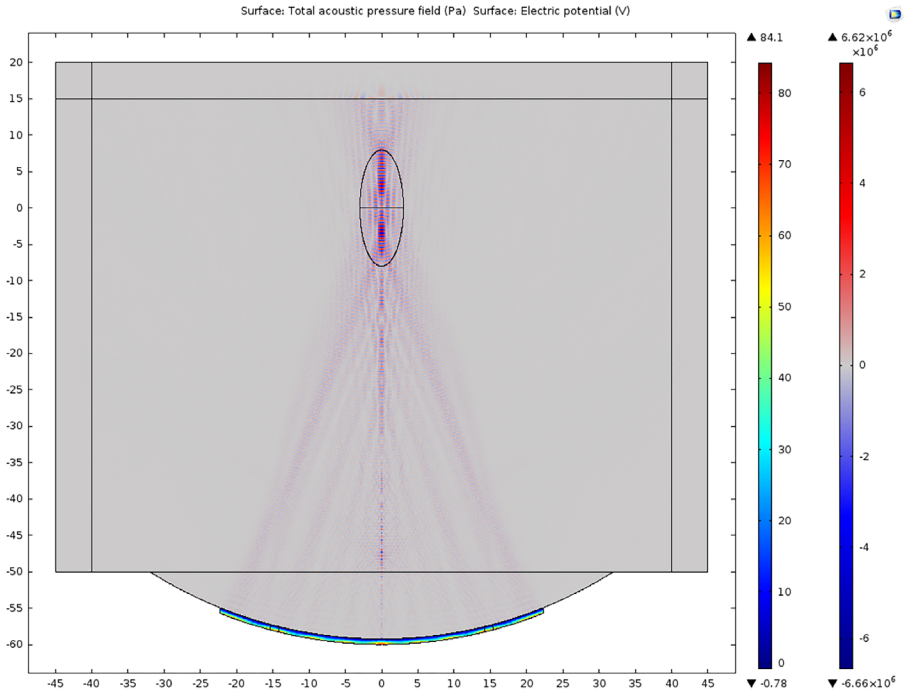

Figure 2. Multiphysics simulation of system. Electric potential profiles of the inner and outer PZT elements (bottom) that emit two acoustic beams into the control volume that focus at a common focal point. The intensity of the acoustic field is given by the rightmost colorbar in Pascals, whereas the PZT electric potential is given by the leftmost colorbarin Volts. The acoustic beams from the elements are directed towards the focal point in the Z (vertical) and X (horizontal) directions.

Reson Inc. Goleta, CA) is used to record the sample's emitted signal. The signal recorded by the hydrophone passes through a low noise amplifier, programmable bandpass filter (SRS 650, Stanford Research Systems, Inc. Sunnyvale, CA), and Lock-in Amplifier. The Lock-in Amplifier improves the rejection of out-of-band noise and increases the dynamic range. The acoustic emission at the difference frequency is filtered out by the LNA. There is a significant increase in the sensitivity to the difference frequency of the target's main emission because other acoustic emissions from the target are filtered. The focused beams from the curved confocal transducer are then raster scanned, point-by-point, over the surface of the target. At each position, the amplitude of the emitted wave is obtained from the Lock-in Amplifier. MATLAB version 2016A (The MathWorks, Inc., Natick, MA) was used to spatially reconstruct the acoustic profile at the difference frequency with each pixel mapped to a spatially-varying, weighted value of the peak amplitude.

Tissue-mimicking Phantoms

Polyvinyl Alcohol (PVA) tissue-mimicking phantoms (TMPs) were fabricated as a model prior to imaging *ex vivo* tissue with the VA system. The PVA TMPs retain acoustic velocities from 1520 to 1540 m/s, which is within the typical range for human soft tissue and characterize the acoustic impedances similar to those of human breast and skin tissue [34–36]. The TMPs were fabricated by placing organic powdered extract (Polyvinyl Alcohol, Sigma-Aldrich, St. Louis, MO) in a beaker with deionized water, followed by repeated mixing while the beaker was placed in a steaming water bath at approximately 90°C. This step ensured sufficient cross-linking between the polymers. The PVA phantom was allowed to solidify and cool for 2 hours before placement into a freezer at -20ºC for 24 hours. After the allotted time, the TMP was removed and allowed to thaw for 2 hours at room temperature, marking the completion of one freezing-thawing cycle. This process is imperative for PVA phantoms to mimic the aforementioned properties of human tissue [37,38]. One rectangular PVA phantom and three spherical phantoms were fabricated for VA scanning. The difference frequency acoustic emissions from the phantoms in each scan were detected and measured using the hydrophone and downstream filter stages as described above. The peak amplitude of acoustic emission was mapped to a weighted pixel value and used to construct an image of the scanned phantom.

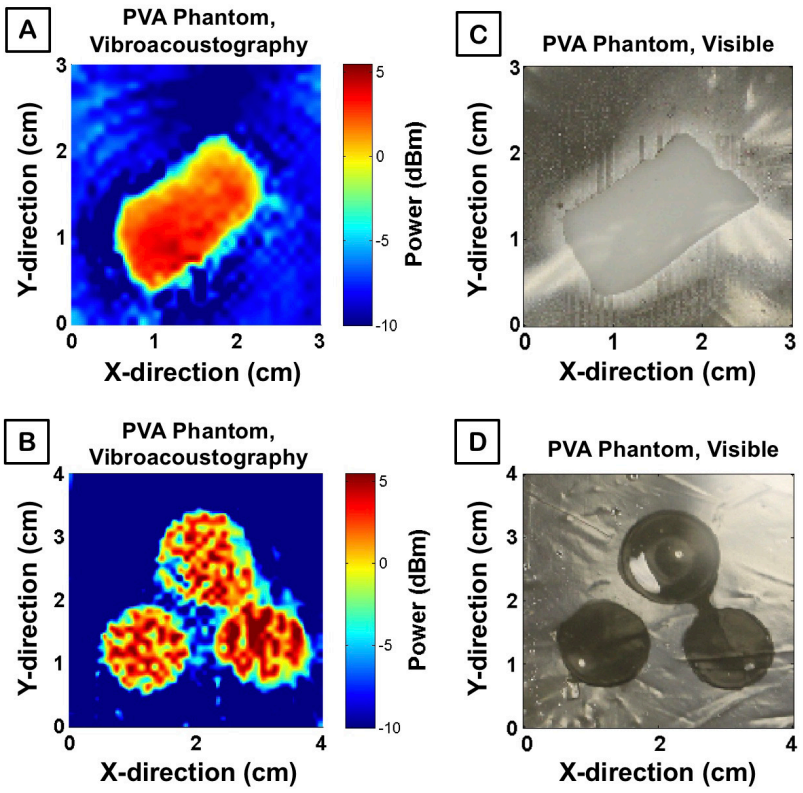

Figure 3. System validation with phantoms. **A**) VA scan of rectangular PVA phantom; pixel color is based on the amplitude of the acoustic emission at the given spatial position within the sample, **B**) VA image of circular PVA phantoms, **C**) High resolution photograph of rectangular PVA phantom in orientation from which the VA image was generated, **D**) High resolution photograph of circular PVA phantoms.

IRB Approval and Protocol

Study approval has been obtained by the institutional review board of the University of California at Los Angeles (IRB#11-002858-CR-00006). Patients undergoing surgical resection for head and neck squamous cell carcinoma were identified on a prospective basis. When a patient presented to clinic with a newly diagnosed lesion and surgery was recommended, the patient was asked for voluntary participation in this study to allow *ex vivo* imaging of his or her specimens with VA after the operation but before routine histopathological analyses. Before surgery, the benefits and risks were discussed with the patient and an opportunity for questions was provided. All patients provided signed written consent for involvement in the study. We did not lengthen the standard procedures the patients received nor did we delay their care for efficacious treatment.

Ex vivo *Specimens*

Two human *ex vivo* OSCC samples were obtained from the Ronald Reagan UCLA Medical Center by Dr. Maie St. John, MD, PhD, Professor and Chair, Department of Head and Neck Surgery at UCLA. Each specimen was resected ensuring the entire tumor and surrounding epithelial and mesenchymal tissues were kept intact. The samples were stored in a saline solution upon transfer to the VA system and the specimens were then scanned. Each tissue sample was first placed in a polystyrene latex sleeve filled with an acoustic scanning gel. This gelled sleeve prevented contamination and facilitated placement of the sample in the ultrasound tank. The gel also served the purpose of reducing the amount of acoustic attenuation at the surface of the tissue. Histological cross-sections were obtained from the department of Pathology and Laboratory Medicine at UCLA following specimen imaging.

RESULTS

System Simulation

We simulated our VA system using COMSOL in order to evaluate the theoretical ARF beam pattern for imaging biological tissue. The simulation results are presented in Figure 2 and demonstrate the pressure intensity emitted from the transducer. The acoustic beams

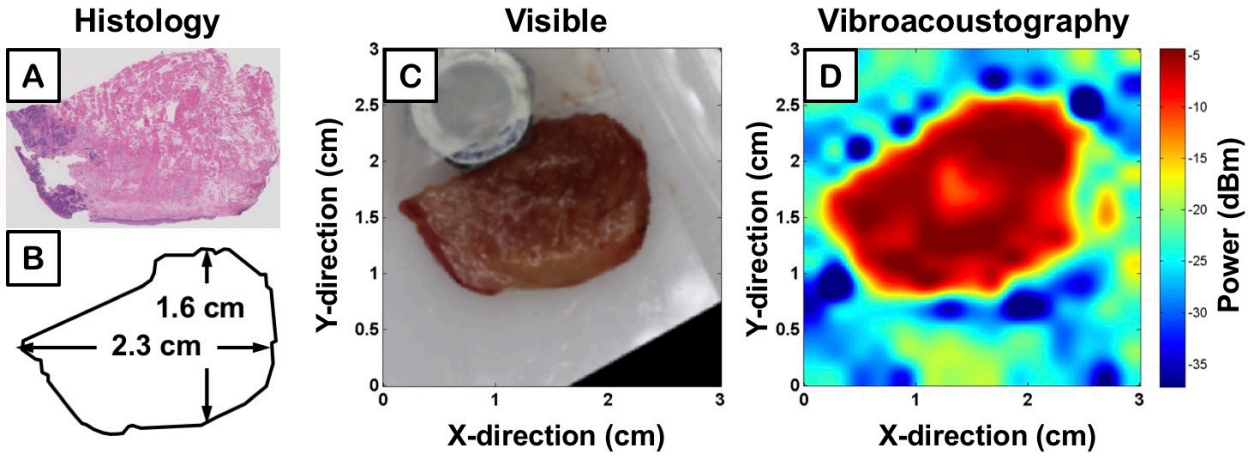

Figure 4. *Ex vivo* image of human tongue with squamous cell carcinoma; first sample. **A**) Histological section of the specimen, **B**) Graphical representation of the specimen, **C**) High resolution visible image of the sample, **D**) VA image of the power of acoustic emission from the sample at 38 kHz represented by colored pixels.

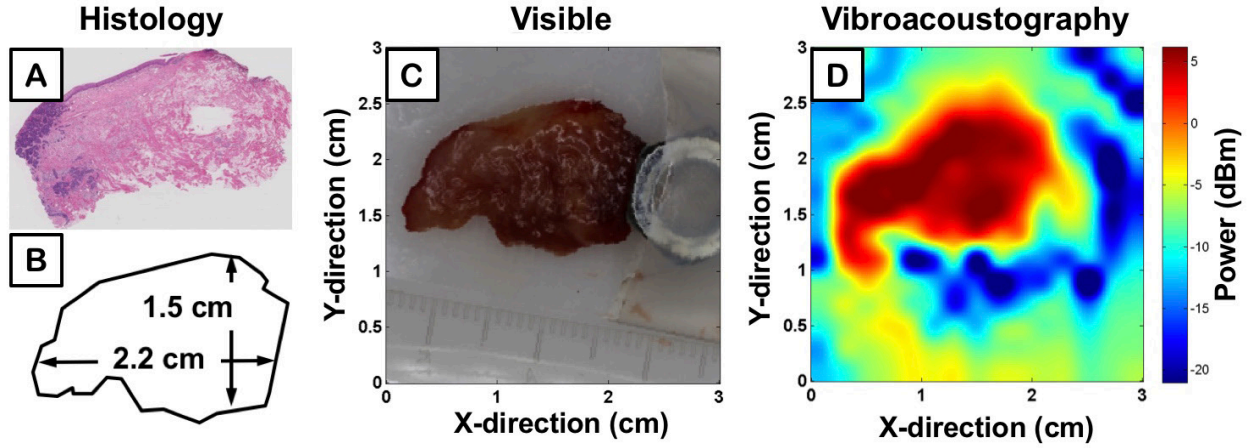

Figure 5. *Ex vivo* image of human tongue with squamous cell carcinoma; second sample. **A**) Histological section of the resected tissue, **B**) Diagram of resected *ex vivo* tissue dimensions, **C**) High resolution photograph of resected *ex vivo* tissue, **D**) VA scan of *ex vivo* tongue reconstructed into a 2D image with VA amplitude measurement.

from each of the elements were offset by a difference frequency of 38 kHz. The intensity of the ARF is focused within an ellipsoid focal volume outlined in Figure 2 with cross-hairs along the axial (Z direction) and lateral (X direction). The acoustic intensity is given in Pascal by the rightmost color bar, whereas the electric potential of the surface of the transducer is displayed in Volts by the left-most color bar. The voltage across each element is within a relatively low regime throughout, supporting the use of our current probe for imaging. The electric field specific to each element produces the desired MHz frequencies by inducing vibration in the crystal structure of the lead zirconate titanate (PZT) elements. This results in the acoustic pulse directed towards the common focal point from each element. The simulation provides the theoretical region of volume where the ARF is able to perturb tissue. The theoretical dimensions of this volume provide an estimate of the amount of tissue that is perturbed by the ARF, which is within the outlined elliptical region. Image resolution can be further estimated based on the ARF dimensions.

Tissue-mimicking Phantoms

The inner and outer elements of the transducer were offset by 38 kHz, the difference frequency of the ARF used to perturb the sample at its surface. The sample was

raster scanned by this ARF in 0.5 mm step-sizes at a sufficiently large field of view to image the entirety of the sample. At each point of the scan, the sample's acoustic emission in response to the ARF was collected by the hydrophone. The signal was then filtered out to obtain the acoustic emission of the specimen at the precise 38 kHz difference frequency by which it was perturbed. The amplitude of the emission from the specimen at each point was then used to construct a spatial image.

Four PVA TMPs were prepared to have similar elastic and acoustic properties as human tissue in order to demonstrate the capacity of the system for *ex vivo* imaging of human specimens. VA-generated images were produced with a false color map labeling the power of acoustic emission generated at each point of the sample (Figures 3A and 3B). The blue and red pixels correspond to low and high sample acoustic intensity, respectively. The corresponding visible images are displayed in Figures 3C and 3D.

Ex vivo *Specimens*

Two specimens of human tongue from different patients with SCC were imaged with the same parameters as TMP experiments. Corresponding histology is displayed in Figures 4A and 5A, while Figures 4B and 5B outline the contour of the photographs displayed in Figures 4C and 5C. The VA-generated image maps of the amplitude of acoustic emission from each sample are demonstrated in Figures 4D and 5D, where blue and red pixel values correspond to low and high power of sample acoustic emission, respectively. The metal nut, seen in Figures 4C and 5C, served as a fiducial marker for an unrelated project and was removed before the tissue was inserted in a polystyrene latex sleeve filled with an acoustic scanning gel and placed within the ultrasound tank for VA-imaging.

DISCUSSION

VA is a non-invasive imaging modality that contrasts tissue regions by identifying disparities in viscoelasticity. This method delivers a radiation force through concurrent emission of two non-destructive low MHz tones, ultimately producing an image of the spatially-varying amplitude and phase elicited as a function of tissues' mechanical properties. In our model we simulated the feasibility of this system and determined the specifications of the acoustic profile emitted from each element and the surface electric potential levels of the transducer. The resulting acoustic profile demonstrated a high-pressure field within a localized field at the focal point of the transducer. The intensity of this ARF proved feasible for the further experiments with tissue samples and *ex vivo* specimens.

The acoustic emission power map acquired from each set of TMPs roughly delineates the boundary between the phantom and the surrounding water. Moreover, each phantom was created as an isotropic, homogeneous substrate, and thus a uniform VA response is expected. Successfully, the rectangular phantom VA image displays relative uniformity in its signal intensity map. The spherical phantoms, although not as uniform, do indeed illustrate a relatively consistent emission throughout. The gaps in the spherical TMP image, however, may be due to the non-ideal axial depth of the VA focal beam, which possesses a spatial cutoff theoretically in the sub-millimeter range. The localized force, thus not yet ideal, may have recorded information from the surrounding water in the imaging tank, rather than the PVA, as the spherical curvature of the phantom leveled off and was replaced by the surrounding media at the imaging plane of the ARF. Despite our current limitations, each phantom is delineated clearly from the surrounding water and supports VA as a promising technique for *ex vivo* and future *in vivo* tumor margin detection.

By comparing quantitative measurements of tissue dimensions (Figures 4B and 5B) to respective VA images (Figures 4D and 5D), our system demonstrates the ability to reconstruct general tissue boundaries that correlate with the actual measurements. Although there is a distinct drop in power amplitude when moving from within the tissue to the surrounding medium, the pixel values are graded; that is, there is not a stark jump from high power acoustic emission of tissue (*i.e*. red) to background (*i.e*. blue). The discrepancy is due to the lateral beam width and side-lobes of the VA transducer, which is theoretically within several hundred microns. Current work is ongoing to characterize this resolution limit. The ability for VA to provide enhanced accuracy in quantitative measurements and more defined boundaries requires the ARF to be within a smaller, more localized volume that perturbs solely the tissue without interfering with the signal through stimulation of neighboring types of background media.

The imaged *ex vivo* specimens also demonstrate differences in VA emission amplitude attributable to differences in viscoelastic properties, specifically elasticity (*i.e*. stiffness), of the respective tissue. The corresponding emitted acoustic field from less elastic tissue is of higher intensity and is represented by high VA amplitudes in the VA images. Tumor lesions have previously been shown to demonstrate highly elastic properties that make their tactile assessment via palpation the standard procedure for current intraoperative identification [39,40]. Figures 4D and 5D demonstrate differences in VA acoustic emission from the different portions of heterogeneous tissue samples containing both tumor and healthy tissue, further

corroborated by the histology sections (Figures 4A and 5A). The VA signal intensity contours identify portions of tumor present in tissue that mirror neoplastic regions in histology.

The reverberations surrounding the tissues in Figures 4D and 5D are likely due to the standing wave effect [31], which were mitigated by the acoustic absorbers lining the ultrasound tank. The polystyrene latex scanning sleeve, however, is believed to augment reverberations when imaging *ex vivo* tissue. The acoustic coupling sleeve was not needed for the TMPs as they could be directly placed in the water tank due to their well-defined boundaries and absence of contamination. The artifacts may also be due to the transducer itself, which generates an internal vibration separate from the two tones for the ARF that is believed to interfere with the acoustic emission of the *ex vivo* tissue.

The significant depth of penetration of VA (*i.e.* ~6 cm in our device) results from the acoustic stress field located at the focal point of the curved transducer. In comparison to water penetration tested herein, tissue attenuation is expected to significantly reduce the penetration depth from 6 cm depending on the tissue composition at the particular area of interest. The *in vivo* focal length of the system is not characterized in this paper, yet the extended focal length of the acoustic stress field is anticipated to aid surgeons in the detection of focal lesions in tissue. Specifically, VA offers 3D imaging of these focal lesions due to its ability to focus an ARF at multiple imaging planes beneath the surface of tissue. The focal length of VA may also be manufactured at precise curvatures to target specific axial distances where suspect tissue may reside. The high depth of penetration may enhance non-invasive detection of deep tissue lesions during future intraoperative procedures. Furthermore, this tool may eliminate the necessity of incisions for endoscopic use of optical techniques that exhibit a shallow depth of penetration.

A challenge to overcome is the design of a phased array with multiple elements for ultra-fast, real-time imaging. In order to precisely quantify small tumors on the order of hundreds of microns that may otherwise be unseen by visual inspection or touch, we would need to image with a smaller, more localized focal volume. Potential solutions include raising the resolution by fabricating a higher quality probe and using lower frequencies to decrease the amount of signal attenuation in tissue. In addition, the difference frequency could be optimized with respect to the imaged tissue. This could be achieved by identifying the viscoelastic properties of the sample and matching these to the difference frequency that produces the highest power response. This aim requires a database of viscosity, elasticity, and time constant values for pertinent biological tissues with corresponding frequencies yielding the highest acoustic emission. Overall, VA is still a novel ultrasonic imaging technique that must undergo further comprehensive testing to validate the displayed quantification of tissue with corresponding histology.

Future directions include: (1) the use of heterogeneous tissue phantoms for resolution characterization and system sensitivity, (2) clinical trial in patient screening and intraoperative guidance during surgical tumor resection, and (3) use of phase images in addition to measurements of amplitude. This tool may prove especially useful towards the localization of tumors or fingers of tumor that are deep within tissue. The complete primary resection of tumors will reduce recurrence and ultimately improve patient outcomes in surgical oncology.

Funding Statement: PAP: UCLA Medical Scientist Training Program (grant T32GM008042), ZDT and WG: Funding from UCLA Henry Samueli School of Engineering and Applied Sciences, Los Angeles, CA, MASJ: Funding from American Academy of Otolaryngology–American Head & Neck Society Surgeon Scientist Career Development Award (MASJ), the Tobacco-Related Disease Research Program of the University of California (MASJ), the STOP Cancer Foundation (MASJ), and the UCLA Henry Samueli School of Engineering and Applied Sciences, Los Angeles, CA.

REFERENCES

1. Lo Nigro C, Denaro N, Merlotti A, Merlano M. Head and neck cancer: improving outcomes with a multidisciplinary approach. Cancer Manag Res. 2017;9:363–71.
2. Wu C, Gleysteen J, Teraphongphom NT, Li Y, Rosenthal E. In-vivo optical imaging in head and neck oncology: basic principles, clinical applications and future directions. Int J Oral Sci. 2018;10(2):10.
3. Mignogna MD, Fedele S, Russo LL. The World Cancer Report and the burden of oral cancer. Eur J Cancer Prev. 2004:13(2):139–42.
4. Aliperti LA, Predina JD, Vachani A, Singhal S. Local and Systemic Recurrence is the Achilles Heel of Cancer Surgery. Ann Surg Oncol. 2011 Mar;18(3):603–7.
5. Mignogna MD, Fedele S, Russo LL, Ruoppo E, Muzio LL. Oral and pharyngeal cancer: lack of prevention and early detection by health care providers. Eur J Cancer Prev. 2001;10(4):381–3.
6. Alldinger I, Yang Q, Gocht A, Raffel A, Knoefel WT, Peiper M. Prognosis and treatment of primary deep soft tissue sarcomas. Anticancer Res. 2007;27(4C):2759–64.
7. Tringale KR, Pang J, Nguyen QT. Image-guided surgery in cancer: A strategy to reduce incidence of positive surgical margins. Wiley Interdiscip Rev Syst Biol Med. 2017 Nov;2018:1–18.
8. Lawaetz M, Homøe P. Risk factors for and consequences of inadequate surgical margins in oral squamous cell carcinoma. Oral Surg Oral Med Oral Pathol Oral Radiol. 2014;118(6):642–6.
9. DiNardo LJ, Lin J, Karageorge LS, Powers CN. Accuracy, utility, and cost of frozen section margins in head and neck

cancer surgery. Laryngoscope. 2000;110:1773–6.
10. Anderson CR, Sisson K, Moncrieff M. A meta-analysis of margin size and local recurrence in oral squamous cell carcinoma. Oral Oncol. 2015;51(5):464–9.
11. Chiosea SI. Intraoperative Margin Assessment in Early Oral Squamous Cell Carcinoma. Surg Pathol Clin. 2017 Mar;10(1):1–14.
12. Shapiro M, Salama A. Margin Analysis: Squamous Cell Carcinoma of the Oral Cavity. Oral Maxillofac Surg Clin North Am. 2017;29(3):259–67.
13. Keereweer S, Van Driel PB, Snoeks TJ, Kerrebijn JD, Baatenburg de Jong RJ, Vahrmeijer AL, et al. Optical image-guided cancer surgery: challenges and limitations. Clin Cancer Res. 2013;19(14):3745–54.
14. Iqbal H, Pan Q. Image guided surgery in the management of head and neck cancer. Oral Oncol. 2016 Jun;57:32–9.
15. Fass L. Imaging and cancer: A review. Mol Oncol. 2008;2(2):115–52.
16. O'Brien WD. Ultrasound-biophysics mechanisms. Prog Biophys Mol Biol. 2007;93(1–3):212–55.
17. McQueen AS, Bhatia KS. Head and neck ultrasound: technical advances, novel applications and the role of elastography. Clin Radiol. 2018;73(1):81–93.
18. Urban MW, Alizad A, Aquino W, Greenleaf JF, Fatemi M. A Review of Vibro-acoustography and its Applications in Medicine. Curr Med Imaging Rev. 2011;7(4):350–9.
19. Maccabi A, Taylor Z, Bajwa N, Mallen-St J. Clair, M. St. John, S. Sung, W. Grundfest and GS. An examination of the elastic properties of tissue-mimicking phantoms using vibro-acoustography and a muscle motor system. Rev Sci Instrum. 2016;87(2).
20. Mazumder D, Umesh S, Vasu RM, Roy D, Kanhirodan R, Asokan S. Quantitative vibro-acoustography of tissue-like objects by measurement of resonant modes. Phys Med Biol. 2016;62(1).
21. Baggio AL, Kamimura HA, Lopes JH, Carneiro AA, Silva GT. Parametric array signal in confocal vibro-acoustography. Appl Acoust. 2017;126:143–8.
22. Fatemi, Mostafa and JFG. Vibro-acoustography: an imaging modality based on ultrasound-stimulated acoustic emission. Proc Natl Acad Sci USA. 1999;96(12):6603–8.
23. Kwon SJ, Jeong MK. Advances in ultrasound elasticity imaging. Biomed Eng Lett. 2017;7(2):71–9.
24. Maccabi A, Shin A, Namiri NK, Bajwa N, John MS, Taylor ZD, et al. Quantitative characterization of viscoelastic behavior in tissue-mimicking phantoms and ex vivo animal tissues. PLoS One. 2018;13(1):1–18.
25. Maccabi A, Garritano J, Arshi A, Saddik G. Tajudeen B a., St. John M, et al. Ex vivo viscoelastic characterization of head and neck tissue abnormalities using ultrasound-stimulated vibro-acoustography (USVA). In: Bosch JG, Doyley MM, editors. 2014. p. 904006.
26. Li GY, Cao Y. Mechanics of ultrasound elastography. Proceedings Math Phys Eng Sci. 2017;473(2199):20160841.
27. Alizad, Azra, Dana H. Whaley, James F. Greenleaf and MF. Potential applications of vibro-acoustography in breast imaging. Technol Cancer Res Treat. 2005;4(2):151–7.
28. Alizad A, Fatemi M, Wold LE, Greenleaf JF. Performance of vibro-acoustography in detecting microcalcifications in excised human breast tissue: A study of 74 tissue samples. IEEE Trans Med Imaging. 2004;23(3):307–12.
29. Yamamoto N, Kinnick RR, Fatemi M, Muraki T, Sperling JW, Steinmann SP, Cofield RH, Itoi E, An K. Diagnosis of small partial-thickness rotator cuff tears using vibro-acoustography. J Med Ultrason (2001). 2015;42(1):3-7.
30. Nogueira-Barbosa MH, Kamimura HA, Braz G, Agnollitto PM, Carneiro AA. Preliminary results of vibro-acoustography evaluation of bone surface and bone fracture. Quant Imaging Med Surg. 2017;7(5).
31. Mitri FG, Greenleaf JF, Fatemi M. Chirp imaging vibro-acoustography for removing the ultrasound standing wave artifact. IEEE Trans Med Imaging. 2005;24(10):1249–55.
32. Namiri NK, Maccabi A, Bajwa N, Badran KW, St. John MA, Taylor ZD, Grundfest WS, Saddik, GN. Identifying viscoelastic parameters of tissue specimens using Hertz contact mechanics. Proc SPIE 10486, Des Qual Biomed Technol XI. 2018.
33. Namiri NK, Maccabi A, Bajwa N, Badran KW, Taylor ZD, St. John MA, Grundfest WS, Saddik, GN. Optimizing signal output: effects of viscoelasticity and difference frequency on vibroacoustic radiation of tissue-mimicking phantoms. Proc SPIE 10484, Adv Biomed Clin Diagnostic Surg Guid Syst XVI. 2018.
34. Zell K, Sperl JI, Vogel MW, Niessner R. Acoustical properties of selected tissue phantom materials for ultrasound imaging. Phys Med Biol. 2007;52(20):N475-84.
35. Cournane S, Cannon L, Browne JE. Assessment of the accuracy of an ultrasound elastography liver scanning system using a PVA-cryogel phantom with optimal acoustic and mechanical properties. Phys Med Biol. 2010;55(19):5965-83.
36. Jiang S, Liu S, Feng W. PVA hydrogel properties for biomedical application. J Mech Behav Biomed Mater. 2011;4(7):1228-33.
37. Cao R, Huang Z, Varghese T, Nabi G. Tissue mimicking materials for the detection of prostate cancer using shear wave elastography: A validation study. Med Phys. 2013;40(2):022903.
38. Wells PN, Liang HD. Medical ultrasound: imaging of soft tissue strain and elasticity. J R Soc Interface. 2011;8(64):1521-49.
39. Das D, Gupta M, Kaur H, Kalucha A. Elastography: the next step. J Oral Sci. 2011;53(2):137-41.
40. Vigneswaran N, Williams MD. Epidemiologic trends in head and neck cancer and aids in diagnosis. Oral Maxillofac Surg Clin North Am. 2014;26(2):123-41.